Zonulae Occludentes in Junctional Complex-enriched Fractions from Mouse Liver: Preliminary Morphological and Biochemical Characterization

BRUCE R. STEVENSON and DANIEL A. GOODENOUGH

Program in Cell and Developmental Biology and Department of Anatomy, Harvard Medical School, Boston, Massachusetts 02115. Dr. Stevenson's present address is Department of Biology, Yale University, New Haven, Connecticut 06511.

ABSTRACT A bile canaliculus-derived preparation containing junctional complexes has been obtained from mouse livers using subcellular fractionation techniques. The junctional complexes include structurally intact *zonulae occludentes* (ZOs). Extraction of this preparation with the anionic detergent sodium deoxycholate (DOC) left junctional ribbons, the detergent-insoluble zonular remnants of the junctional complexes. When visualized in negative stain electron microscopy, each of these ribbons contained a branching and anastomosing network of fibrils which appears similar to that of ZOs in freeze-fractured whole liver. Comparative measurements of freeze-fracture and negative stain fibril diameters and network densities support this relationship. SDS polyacrylamide gel analysis shows the DOC-insoluble junctional ribbons to be characterized by major polypeptides at 37,000 and at 48,000, with minor bands at 34,000, 41,000, 71,000, 86,000, 92,000, and 102,000. The ZO-containing membrane fractions have been isolated in the presence of EGTA in concentrations and under conditions shown by others to disrupt normal ZO morphology and physiology in whole living epithelia. The network of fibrils visualized in these fractions by negative staining is structurally resistant to treatment with DOC, but is either solubilized or disrupted by *N*-lauroylsarcosine.

The *zonula occludens*, or tight junction, represents the transepithelial permeability barrier of the paracellular pathway in most vertebrate epithelia. This intercellular junction forms a gasket-like seal that encircles the cell at the intersection of the apical and lateral plasma membranes, joining each cell to its neighbors, and thus limiting the diffusion of substances between lumenal and serosal compartments. The *zonula occludens* (ZO)[1] was originally described by Farquhar and Palade (1963) as the most apical member of a family of intercellular junctions collectively called the junctional complex. In addition to the ZO, the junctional complex contains the *zonula adhaerens* (intermediate junction, belt desmosome) immediately basal to the ZO, and intermittent desmosomes (*maculae adhaerentes*).

In thin section electron microscopy the ZO appears as a series of punctate membrane "kisses" where the extracellular space is eliminated. The movement of extracellular electron-dense tracer molecules is restricted by these points of membrane contact (15, 18, 25, 44). Electrophysiological studies however, have demonstrated that the ZO is the site of passive transepithelial ion movement (19, 20), the so-called paracellular shunt, indicating that the ZO exhibits selective permeability properties.

Work in several laboratories has shown that normal epithelial structure and function are reversibly disrupted by the chelation of extracellular calcium (6, 7, 9, 16, 21, 31, 42, 43, 51). Exposure of epithelial layers to millimolar concentrations of EGTA or EDTA causes a rapid decrease in transepithelial resistance, a parameter determined largely by the paracellular pathway. Although some investigators did not observe any alteration in ZO ultrastructure under calcium-chelating conditions (3, 6, 51), others reported an ED- or EGTA-induced disruption of ZO structure, visible in both thin section (7) and freeze-fracture (21, 42, 43), leading to the general belief that Ca^{2+} is integrally involved in the stabilization of ZO structure.

[1] *Abbreviations used in this paper:* DOC, deoxycholate; K-PT, potassium phosphotungstate; SRK, *n*-lauroyl sarcosine; UrAc, uranyl acetate; ZO, zonula occludens.

THE JOURNAL OF CELL BIOLOGY · VOLUME 98 APRIL 1984 1209-1221

Following glutaraldehyde fixation, the ZO appears in freeze-fracture replicas as a branching and anastomosing network of continuous P-face fibrils and E-face grooves that correspond to the points of contact seen in thin section (25, 39, 56, 57). In the absence of glutaraldehyde fixation, the ZO is instead seen as a linear series of individual intramembranous particles (57, 59, 60, 61). Recent studies have shown that trypsinized MDCK cells do not form ZOs when plated in the presence of cycloheximide, a protein synthesis inhibitor (30). Combined, these data suggest that the fibrils are composed of protein. Recently a model has been proposed that visualizes the ZO fibril as an inverted cylindrical lipid micelle (35, 49). However, in the absence of more detailed biochemical information, questions regarding the molecular nature of the ZO have remained unresolved.

The ZO is a morphologically and functionally differentiated region of the plasma membrane theoretically susceptible to isolation by subcellular fractionation techniques, as has been done for the gap junction (2, 11, 26, 28, 38) and the desmosome (10, 29, 52). Mammalian liver is an advantageous starting point for ZO isolation because of its large area of ZOs, the large amounts of accessible tissue, and the availability of procedures for the isolation of a bile canaliculus-enriched plasma membrane fraction (47). ZOs have been observed in preparations of isolated hepatocyte plasma membranes since the early 1960s (13, 47). In later years, Goodenough and Revel (25) further characterized the ZO in isolated liver membrane fractions with thin section electron microscopy, and observed the unique branching fibril morphology of the ZO in negatively stained membrane fractions treated with deoxycholate (DOC). These authors concluded that the ZO was soluble in DOC: the negatively stained images found, such as in Fig. 9, were rare, and they were unable to preserve any recognizable ZO structure in thin sections prepared subsequent to DOC treatment. This interpretation has proved not only to be incorrect but has hampered efforts at ZO isolation, since it has been subsequently assumed that selective detergent fractionation is not a viable strategy for ZO enrichment.

In this paper, we re-examine these assumptions and find them to be incorrect. Indeed, the two reagents reported in the literature to be disruptive of ZO structure and function, DOC and EGTA, respectively, are used in combination to dissolve selectively nonjunctional membranes and yield a preparation highly enriched in junctional complexes, notably the detergent insoluble components of the *zonula occludens* and the *zonula adhaerens*. In particular, the negatively stained images of ZO fibrils, reported by Goodenough and Revel (25), are shown not to be rare observations, but present in abundance in these fractions, and this method is established as a reproducible morphological assay that will be essential for the future enrichment of the ZO.

MATERIALS AND METHODS

All reagents were purchased from Sigma Chemical Co. (St. Louis, MO) unless otherwise stated.

ZO Isolation Protocol

LIVER PLASMA MEMBRANES: A bile canaliculus-enriched plasma membrane fraction was isolated by a modification of the techniques of Neville (1960 [47]), Emmelot et al. (1964 [13]), and Song et al. (1969 [55]). White CD-1 mice weighing 27–30 g, 49-d old, and of either sex were purchased from Charles River Breeding Laboratories (Wilmington, MA). The livers from 100 mice were used as starting material. Animals were sacrificed, five at a time, by cervical dislocation, and the livers dissected immediately and homogenized in a 40-ml Bellco Dounce tissue homogenizer (Bellco Glass, Inc., Vineland, NJ), 10 strokes with a loose pestle, in ice-cold 1 mM $NaHCO_3$, pH 8.0 (bicarbonate buffer [BB]). The homogenate was added immediately to 3 liters BB with stirring. All solutions and centrifuge spins prior to the detergent extractions were at 4°C. The pooled and diluted homogenate was allowed to sit on ice for 10 min, filtered through 32 layers of cheesecloth, and spun for 10 min at 2,000 *g* in a Beckman JA-10 rotor (Beckman Instruments, Inc., Spinco Div., Palo Alto, CA) with the centrifuge brake turned off. Centrifugations presented here are calculated from average gravity values of the rotor used. The supernatant solution was discarded, being careful to aspirate off the white fatty material floating on the surface, and the soft upper pellets were gently resuspended by swirling the bottles, discarding the hard white lower pellet. All resuspensions throughout the protocol were performed so as to minimize shear forces. The suspension was diluted to 1 liter with BB, and spun again 10 min at 2,000 *g* in a JA-10 rotor with the brake off. The supernatant solution was discarded, the pellets resuspended to 300 ml with BB. 67% sucrose (wt/wt) in 1 mM $NaHCO_3$, 1 mM EGTA, pH 8.0 was slowly added with stirring until the final sucrose concentration was 50%. This was loaded into the Beckman Ti-15 zonal rotor in a 25-41-50% step gradient, and spun 2 h at 76,000 *g*. The 25-41 interface was collected and allowed to sit overnight on ice in the cold room.

The specimen was diluted to 1 liter with 10 mM Imidazole, 1 mM EGTA, 0.02% azide (M) and spun 20 min at 19,100 *g* in a Beckman JA-14 rotor. The supernatant solution was discarded and the pellets washed twice with 500 ml M (10 min, 2,600 *g*, JA-14 rotor), with care taken to discard the hard white lower pellet after each spin, and once with 120 ml M (10 min, 2,600 *g*, Beckman JA-20 rotor). This bile canaliculus fraction was resuspended in 40 ml M for a gel sample.

In one experiment, aliquots of the canaliculus-enriched fraction were resuspended in M and incubated in a 37°C water bath for 15 and 30 min, and then prepared for electron microscopy as detailed below.

DETERGENT EXTRACTIONS: All manipulations were at 15°C. The pelleted canaliculus-enriched fraction was resuspended in 40 ml M. While stirring, 40 ml 1.0% sodium deoxycholate (DOC) in 10 mM Imidazole, 1 mM EGTA, 0.02% azide was slowly added, and the samples spun 10 min at 11,300 *g* in a JA-20 rotor. The supernatant solution was discarded after a gel sample was made, and the pellets washed 3 times in 60 ml 0.5% DOC in 10 mM Imidazole, 1 mM EGTA, 0.02% azide (MD) (10 min, 2,600 *g*, JA-20 rotor), saving and setting aside the supernatant solution after each spin. The pellets were discarded and the supernatants pooled and washed once with 30 ml MD (10 min, 11,300 *g*, JA-20 rotor). This DOC-insoluble fraction containing the junctional ribbons was resuspended in 4 ml MD for a gel sample.

Pelleted DOC-insoluble samples were resuspended in 4 ml 1.0% *N*-lauroylsarcosine (SRK) (Sarkosyl NL-97, CIBA-Geigy Corp., Ardsley, NY) in 10 mM Imidazole, 1 mM EGTA, 0.02% azide (MS) and spun 10 min at 11,400 *g* in a JA-20 rotor. A gel sample was taken from the supernatant solution before it was discarded and the pellets washed twice with 5 ml MS (10 min, 11,300 *g*, JA-20 rotor), yielding the SRK-insoluble fraction. This was resuspended in 2.0 ml MS for a gel sample.

Throughout the isolation protocol fractions were monitored for purity and efficiency of extraction by phase-contrast light microscopy. Protein determinations were made according to the method of Lowry et al. (1951 [41]).

Electron Microscopy

Fractions were prepared for thin section by centrifugation in a Beckman SW-41 rotor, using BEEM hemihyperboloid polyethylene capsules (Ladd Research Industries, Inc., Burlington, VT, cat. no. 2323) in Epon centrifuge adapters (27). The samples were fixed in 2.0% glutaraldehyde in 0.1 M phosphate buffer pH 7.0 with or without 0.2% tannic acid (1) for 30 min at room temperature, washed with 0.1 M phosphate buffer, postfixed in unbuffered 1.0% OsO_4-1.5% potassium ferrocyanide (37) 1 h on ice, washed with distilled water (dH_2O), dehydrated, and embedded. Thin sections of the pellets were cut parallel to the direction of centrifugation to ensure visualization of all elements in the fraction, and stained with lead citrate. Whole liver tissue was prepared for thin sectioning by immersing minced tissue in Karnovsky's fixative (36) in 0.1 M sodium cacodylate buffer pH 7.4 for 60 min at room temperature, followed by the same protocol detailed above.

Some samples were removed after the primary fixation, equilibrated with glycerol in 0.1 M cacodylate buffer pH 7.4, and frozen in a liquid nitrogen-cooled Freon-22 slurry. Samples were fractured in vacuo at −115°C and shadowed with platinum-carbon in a Balzers BAF301 freeze-fracture device (Balzers High Vacuum Corp., Nashua, NH). Tissue was digested with household bleach and the resultant replicas washed extensively with dH_2O.

For negative staining, small droplets of the DOC- and SRK-insoluble suspensions were applied to glow-discharged carbon/formvar-coated grids, washed

gently with dH_2O, and stained with either 1.0% potassium phosphotungstate (K-PT) at pH 7.0 or 1.0% aqueous uranyl acetate (UrAc) at pH 4.5.

Specimens were viewed in a Siemens Elmiskop 101 (Siemens Corp., Iselin, NJ) at 80 kV. A standard calibration grid (1,134 lines/mm) was used to determine micrograph magnification.

Gel Electrophoresis

11% SDS polyacrylamide slab gels (0.75 × 14.1 × 13.4 mm) were prepared and run according to the methods of Laemmli (1970). Gel samples were made by combining 9 vol of sample with 1 vol 10 × sample buffer while vortexing, and immediately boiling for 2 min. Sample buffer contained 1% 2-mercaptoethanol, 1.3 mM Tris pH 6.8, 0.9% SDS (BDH Chemicals, Ltd., Poole, England), and 0.025% bromophenol blue (final concentrations). Gels were run at 25 mA until 200 V was reached, and at constant voltage thereafter or at 60 V overnight. Staining of gels with Coomassie Blue was according to Fairbanks et al. (1971 [14]), except that staining solution 2 was omitted. Molecular weights were determined by comparison with reduced and alkylated standards run with each gel.

Morphometry

Fibril diameter was measured normal to the ZO long axis on randomly selected freeze-fracture and negative stain electron micrographs using an ocular micrometer. Network density in freeze-fractured and negatively stained specimens was determined according to the method of Easter et al. (1983 [12]) using a MOP-3 Digital Analyzer (Carl Zeiss, Inc., Oberkochen, West Germany). Network density is the total length of fibril elements divided by the length of the canaliculus bordered by the measured fibril pattern. Statistical significance was determined by the student's t test.

RESULTS

Isolation Protocol

The protocol for isolating junctional complex-enriched fractions from mouse liver is diagrammed in Fig. 1. Starting with 180–220 g (wet weight) of liver the final yield of DOC-insoluble material is 6–10 mg total protein, and 2–3 mg of the SRK-insoluble fraction. Variations in the yield can be attributed to the age of the animals, the efficiency of the detergent extractions, and the amount of contaminating material derived from tissue collagen and other as of yet undetermined sources. Younger mice gave a smaller final yield and older mice presented more of a problem with collagen contamination. The livers from larger mammals were not used because of their high collagen content. Successful detergent extractions were critically dependent on temperature and the centrifuge spin sequence used. EGTA was included in all solutions after the first homogenate to prevent clumping, and to produce a better gradient separation and detergent extraction.

Morphology of the Isolated Liver Fractions

Whole liver contains an extensive network of bile canaliculi, the lumena of which are sealed from the blood space by ZOs. These ZOs can be found in their obligatory location on either side of the canalicular lumen as part of the junctional complex (Fig. 2). These ZOs act to separate the bile contents from the intercellular and blood spaces. Whole bile canaliculi and their accompanying junctional complexes occasionally remain morphologically intact following isolation of mouse liver plasma membranes by a modifiction of the Neville technique (1960 [47]) (Fig. 3). Following the protocol outlined in Materials and Methods, most of the bile canaliculi have fragmented, leaving the junctional complexes, attached plasma membranes, and gap junctions connected in pairs of membrane sheets. Fracture faces of these membrane sheets (*inset*, Fig. 3) reveal the characteristic branching and anastomosing

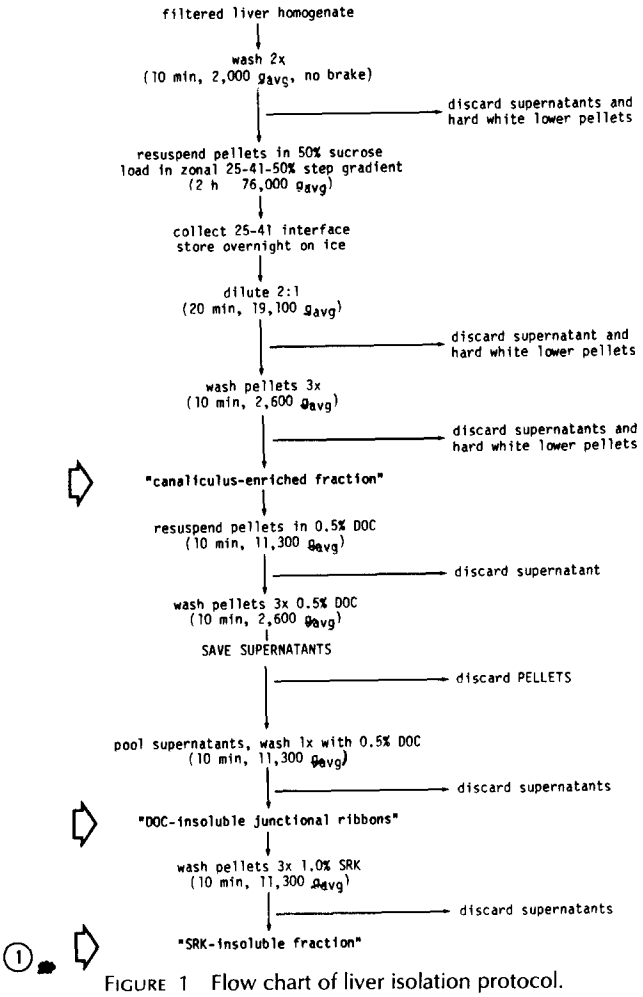

FIGURE 1 Flow chart of liver isolation protocol.

network of ZO fibrils, and occasional associated gap junction connexon arrays. In comparison to whole liver (compare *inset*, Fig. 3 to Fig. 4), the ZO fracture faces appear unchanged following isolation and exposure to low ionic strength buffers and millimolar EGTA, even following incubation with EGTA for up to 30 min at 37°C (data not shown). In Fig. 4, note that in whole liver the ZO depth, fibril number and branching pattern vary significantly over the course of the junction. In this glutaraldehyde-fixed preparation the ZO fibrils appear as continuous ridges.

The detergent sodium deoxycholate (DOC) solubilizes the large majority of liver membranes and leaves behind the junctional complex-associated cytoplasmic density, best seen with negative stain electron microscopy. The specimen shown in Fig. 5 was washed briefly with DOC directly on the grid and then negatively stained with K-PT. Here, a partially solubilized lumenal membrane of the bile canaliculus remains flanked by a pair of junctional complexes that include the ZO fibril network. Following the exhaustive DOC solubilization procedure described in Materials and Methods, the lumena of the bile canaliculi are completely solubilized, leaving long ribbon-like zonular remnants of the junctional complex (Fig. 6). Close examination of these junctional ribbons stained with either K-PT (Fig. 7) or UrAc (Fig. 8) shows that most still contain a branching and anastomosing network of stain-excluding fibrils, which is strongly reminiscent of the patterns of fibrils seen in freeze-fractured whole liver ZOs (compare Figs. 7 and 8 with Fig. 3 [*inset*] and Fig. 4).

The process of detergent solubilization of the hepatocyte lateral membranes can also be followed in thin sections. Prior to detergent extraction, the junctional complexes treated with low salt and EGTA are seen as pairs of plasma membranes, with the focal membrane interactions characteristic of the ZO (Fig. 9). The cytoplasmic surfaces of these membranes are festooned with a dense fuzzy layer of unknown composition in addition to fine filaments. This dense fuzzy layer is insoluble in high salt, alkaline pH, and urea (data not shown). Following treatment with sodium deoxycholate (DOC), most membranes in the preparation are solubilized. Figs. 10 and 11 reveal that the junctional complex membrane has been partially solubilized by DOC, leaving intact portions of the ZO membrane bilayers in addition to the junctional complex-associated cytoplasmic density. This cytoplasmic density appears coarsely clumped following detergent treatment. Based solely on this morphological observation it is difficult to assess the degree of solubilization of cytoplasmic density components or the associated fine filaments. The presence of trilaminar membrane profiles remaining in the region of the ZO is variable. Occasionally almost intact-appearing ZOs remain (Fig. 10), whereas in other ribbons the ZO membranes appear disrupted (Fig. 11) or completely missing. Freeze-fracture of these DOC-treated ribbons have yielded no fracture faces; all of the fracture faces exposed appear either as smooth surfaced, nonparticulate vesicles with no features characteristic of plasma membrane structure, or show the connexon arrays of gap junctions (data not shown).

When the DOC-ribbons are further treated with *N*-lauroylsarcosine (SRK), another anionic detergent, the long ribbon structures and gap junctions remain in the insoluble pellet (Figs. 12–14). In thin section (Fig. 12), SRK does not detectably alter the residual cytoplasmic densities beyond the changes already described for the DOC treatment, and trilam-

---

FIGURES 2 and 3 Fig. 2: In whole liver, *zonulae occludentes* (*ZO*) are found in an obligatory location immediately adjacent to the bile canaliculi. The ZOs are characterized by a series of punctate membrane fusions, with a dense feltwork of fine fibrillar material applied to the cytoplasmic surfaces (arrows). Bar, 100 nm. × 100,000. Fig. 3: Following subcellular fractionation, "intact" bile canaliculi can be found, still flanked by pairs of ZOs in their juxtacanalicular positions. A dense material is seen applied to the cytoplasmic surfaces of the junctional membranes, in addition to fine filaments (arrows). × 71,000; bar = 100 nm. (*inset*) Freeze-fracture replicas of isolated membranes reveal the characteristic branching and anastomosing network of P-face fibrils (closed arrowheads). Gap junctions are found on the lateral membranes and interspersed among the ZO fibrils (open arrows). Bars, 100 nm. × 71,000; × 80,000 (*inset*).

FIGURES 4 and 5 Fig. 4: Freeze-fracture replicas of whole liver provide surface views of the ZOs bordering the lumena of bile canaliculi. The network of P-face fibrils (black arrows) and E-face grooves (white arrows) forms a continuous belt at the edges of the canaliculus. Gap junctions (*GJ*) are found in association with the ZO network. Bar, 100 nm. × 80,000. Fig. 5: Whole liver membranes were adsorbed to carbon/formvar-coated grids, washed with 0.5% DOC, and then negatively stained with 1.0% K-PT. This partial solubilization with DOC leaves the geometry of the canaliculus intact. The lumen of the canaliculus is seen flanked by its junctional complexes (white brackets) which are composed of the bands of cytoplasmic density and a network of stain-excluding fibrils (arrows). Following exhaustive solubilization in DOC, these junctional complexes, or ribbons, remain partially insoluble in the detergent, whereas the membranes of the canalicular lumen and lateral surfaces are solubilized. Bar, 500 nm. × 34,000.

FIGURES 6–8 Fig. 6: Following exhaustive treatment with 0.5% DOC and 1 mM EGTA, the remainder of the junctional complexes are visualized as 0.5–1.0 μm wide ribbons (between arrows) when negatively stained with 1.0% K-PT. These junctional ribbons correspond to the junctional complexes indicated by the white brackets in Fig. 5. The ribbons are very sensitive to shear, and are in varying lengths, occasionally branching, following subcellular fractionation. Bar, 1.0 μm. × 12,500. Fig. 7: A higher magnification view of a junctional ribbon following negative staining in 1.0% K-PT reveals a branching and anastomosing network of stain-excluding fibrils (arrows), reminiscent of fibrils exposed on fracture faces of ZOs. The stain-excluding fibrils are embedded in the amorphous cytoplasmic dense layer, which shows varying degrees of disruption along the length of the junctional ribbons. The stain-excluding fibrils appear of varying thickness, occasionally resolving into tight clusters of several fibrils (black arrow). Bar, 200 nm. × 60,000. Fig. 8: The stain-excluding branching and anastomosing fibrils (arrows) can also be visualized when negatively stained with 1.0% UrAc. As several fibrils converge, thick regions are generated (black arrow); similar thick regions of convergence are seen on freeze-fractured fibrils (*inset*, Fig. 11). Fibrils (open arrow) are significantly wider in UrAc than those visible in K-PT (see Table I). Bar, 100 nm. × 107,000.

FIGURES 9–12 Thin section electron micrographs of centrifuge pellets from liver fractions. Fig. 9 shows the junctional complex with its ZO in a canaliculus-enriched fraction prior to detergent treatment (similar to Fig. 3). On their cytoplasmic surfaces, the junctional membranes have a closely applied dense layer (arrowheads) and associated fine filaments (arrows). Gap junctions (*GJ*) are characteristically free of the dense layer. Figs. 10 and 11 show residual junctional ribbons following treatment with DOC. The cytoplasmic dense layers usually remain in tandem pairs (between arrows). In the region of the *ZO*, pairs of trilaminar membranes are seen in variable amounts. When these pairs of trilaminar membranes associate to form pentalaminar structures, they appear 1.5–2.0 nm narrower in overall width and lack the dense cytoplasmic junctional membrane leaflet of the gap junctions (*GJ*). Fig. 12 shows a junctional ribbon following further extraction of the DOC-treated ribbons with SRK. No apparent changes in the pairs of cytoplasmic dense layers are evident (between arrows), and pairs of trilaminar membranes are still visible in the region of the *ZO*. Gap junctions (*GJ*) are evident and provide a marker for the hepatocyte lateral plasma membranes. Bars, 50 nm. × 130,000.

FIGURES 13 and 14 Fig. 13: Following treatment of DOC-extracted junctional ribbons with SRK, negative staining with K-PT reveals that the ribbons are still intact (between solid arrows). Gap junctions (open arrows) remain associated with the ribbons, and mark their ablumenal or noncanalicular edges. Bar, 1 μm. × 14,200. Fig. 14: At higher magnification, negative staining with K-PT reveals the cytoplasmic dense layer of the junctional ribbon to be devoid of the network of stain-excluding fibrils. A gap junction identifies the ablumenal edge of the junctional ribbon. The asterisks mark the adlumenal edge, at which the fibril network is seen in ribbons treated only with DOC. Bar, 100 nm. × 68,000.


ZO
bile
canaliculus
ZO
2

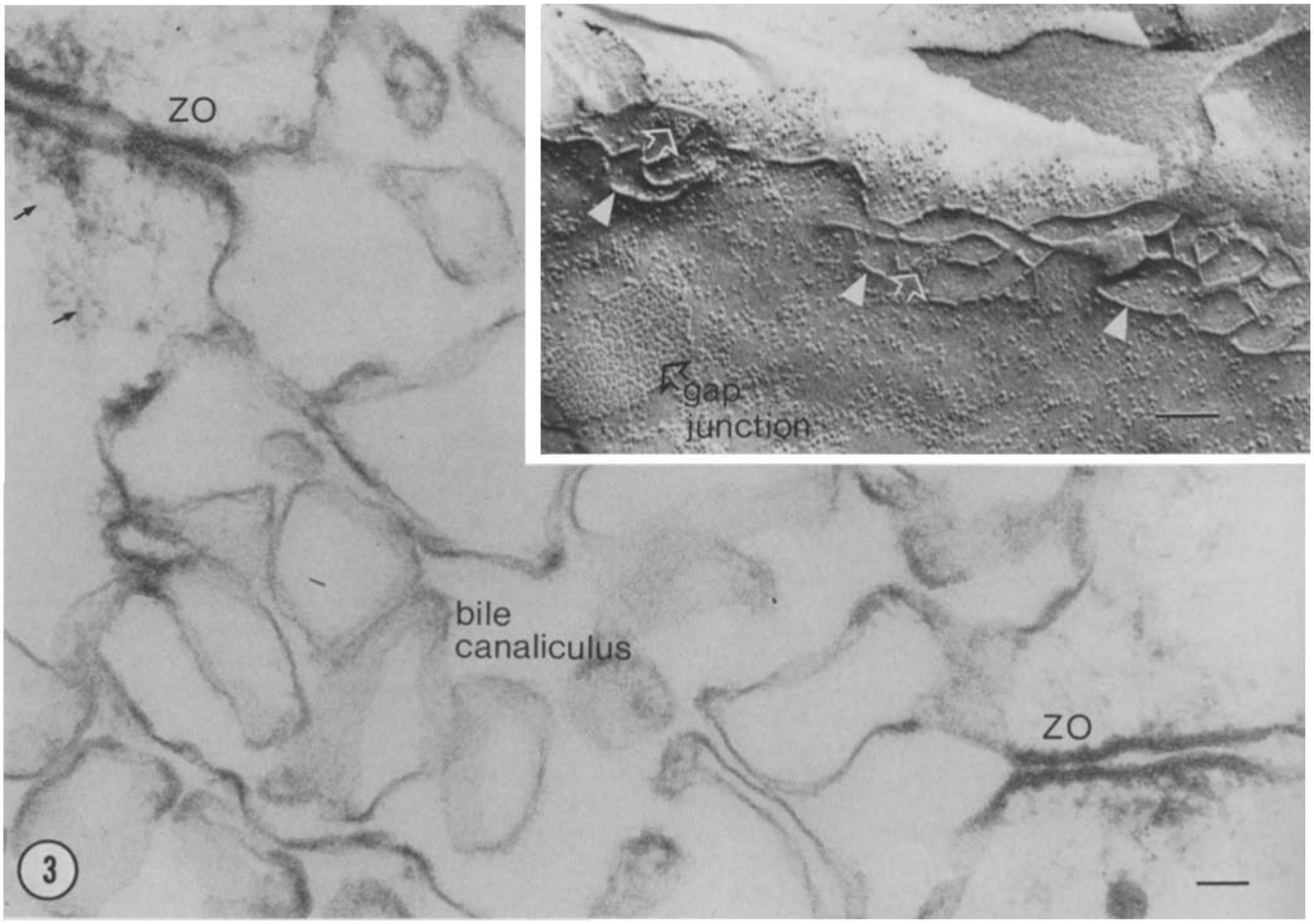
ZO
gap
junction
bile
canaliculus
ZO
3

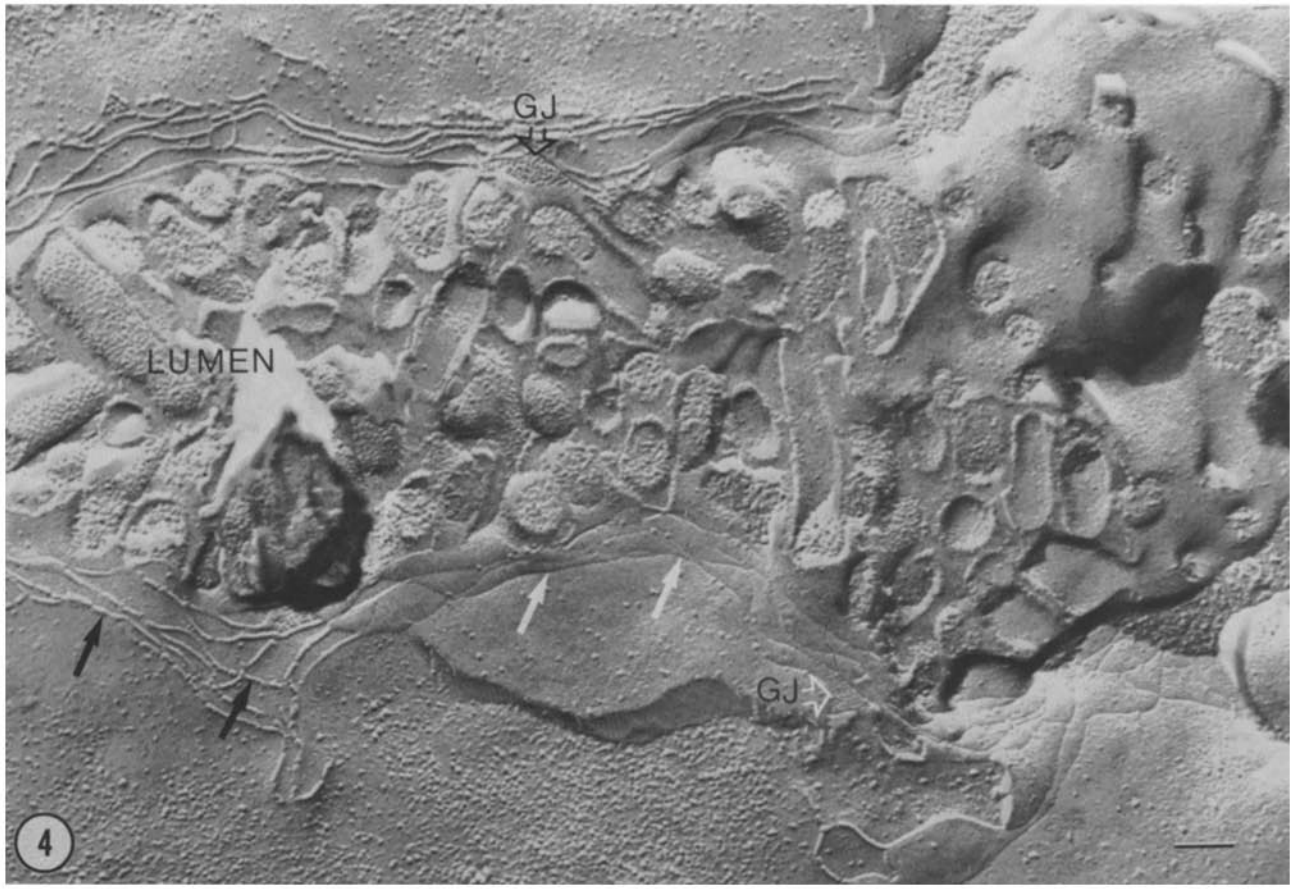
GJ
LUMEN
GJ
4

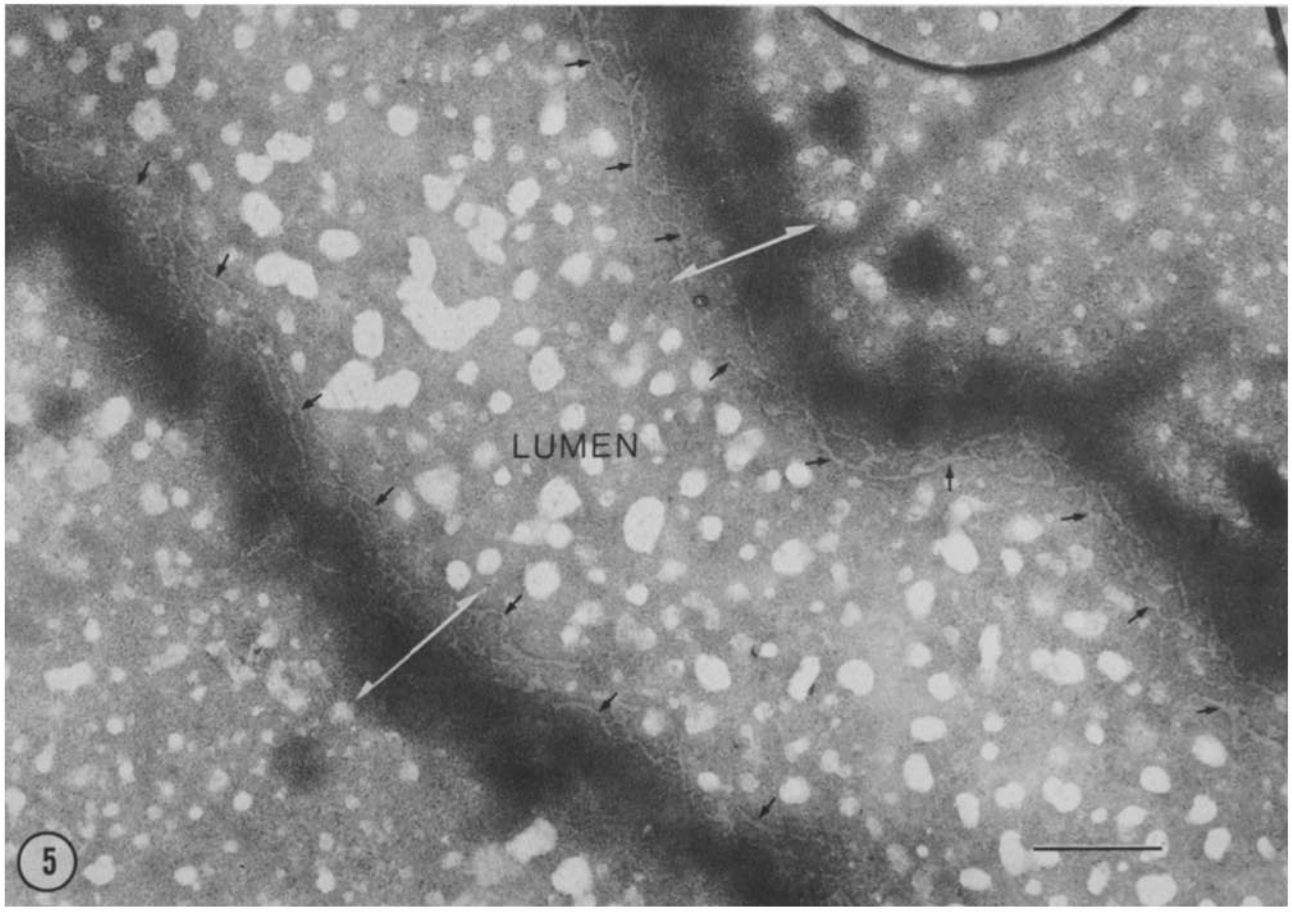
LUMEN
5

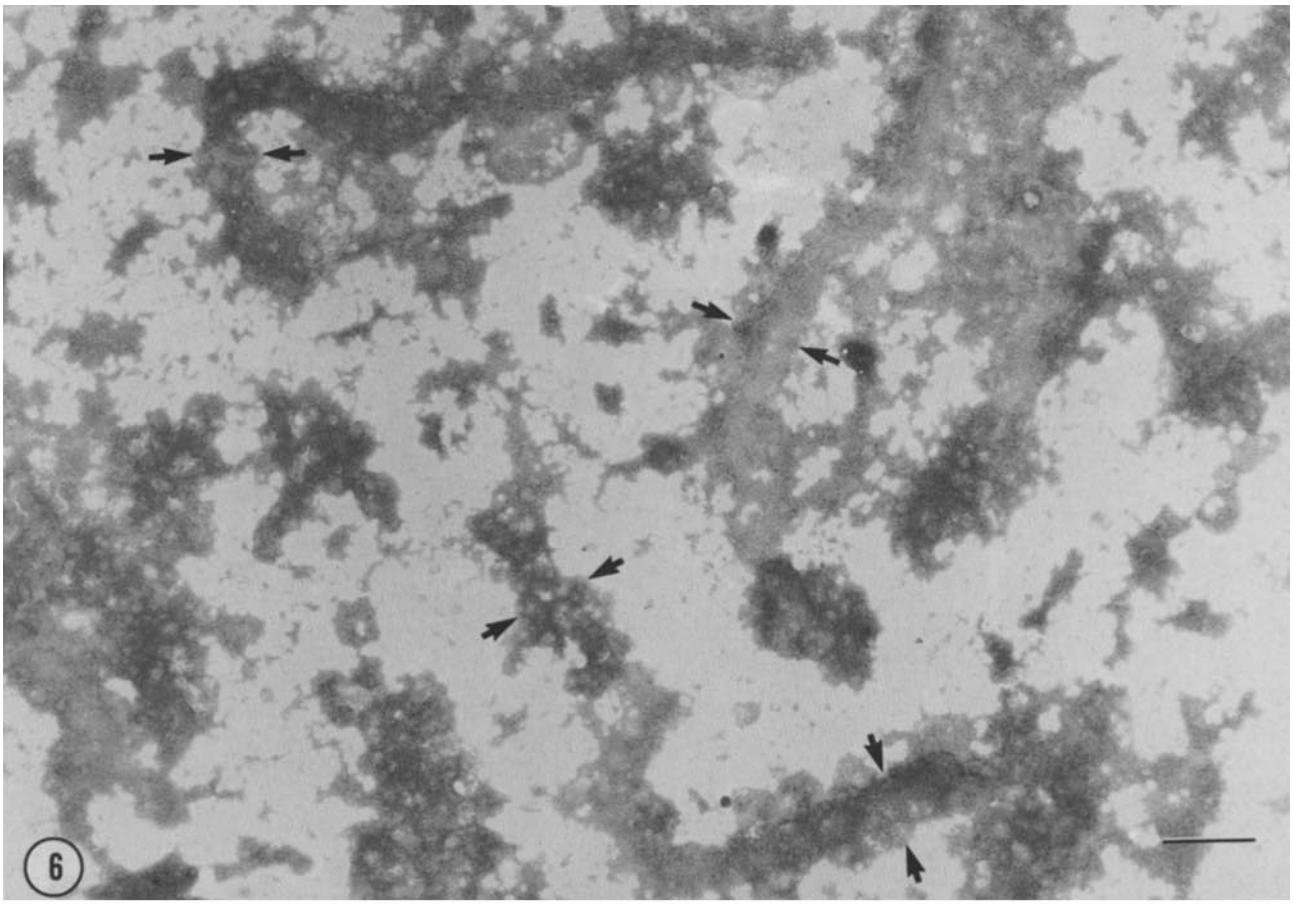
6

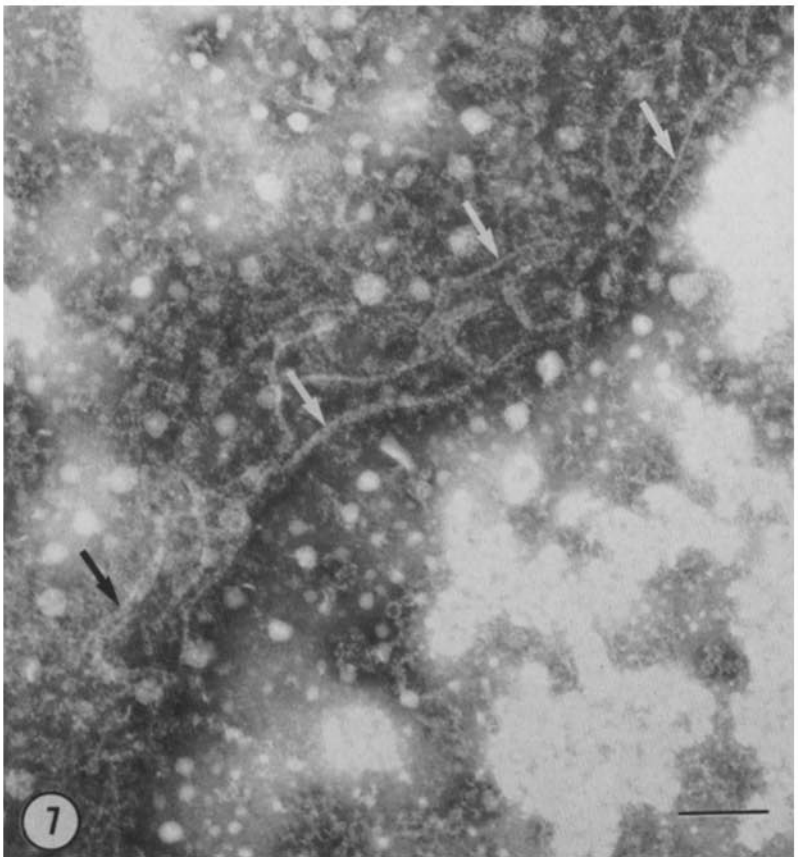
7

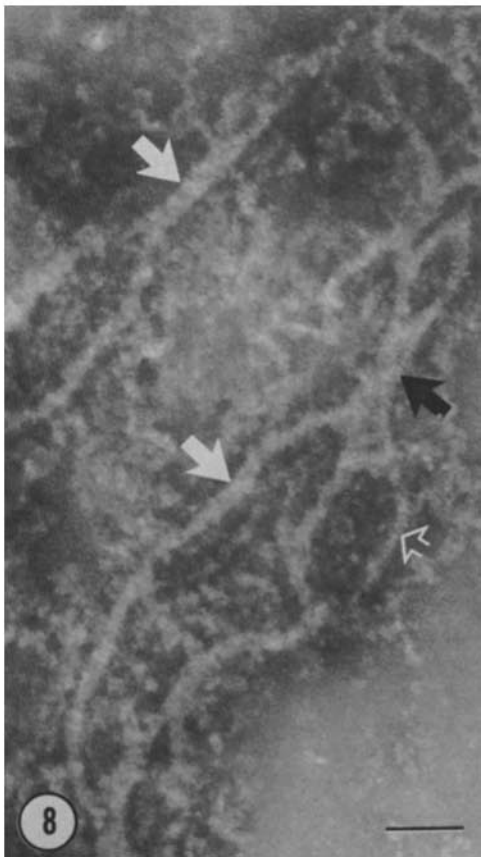
8

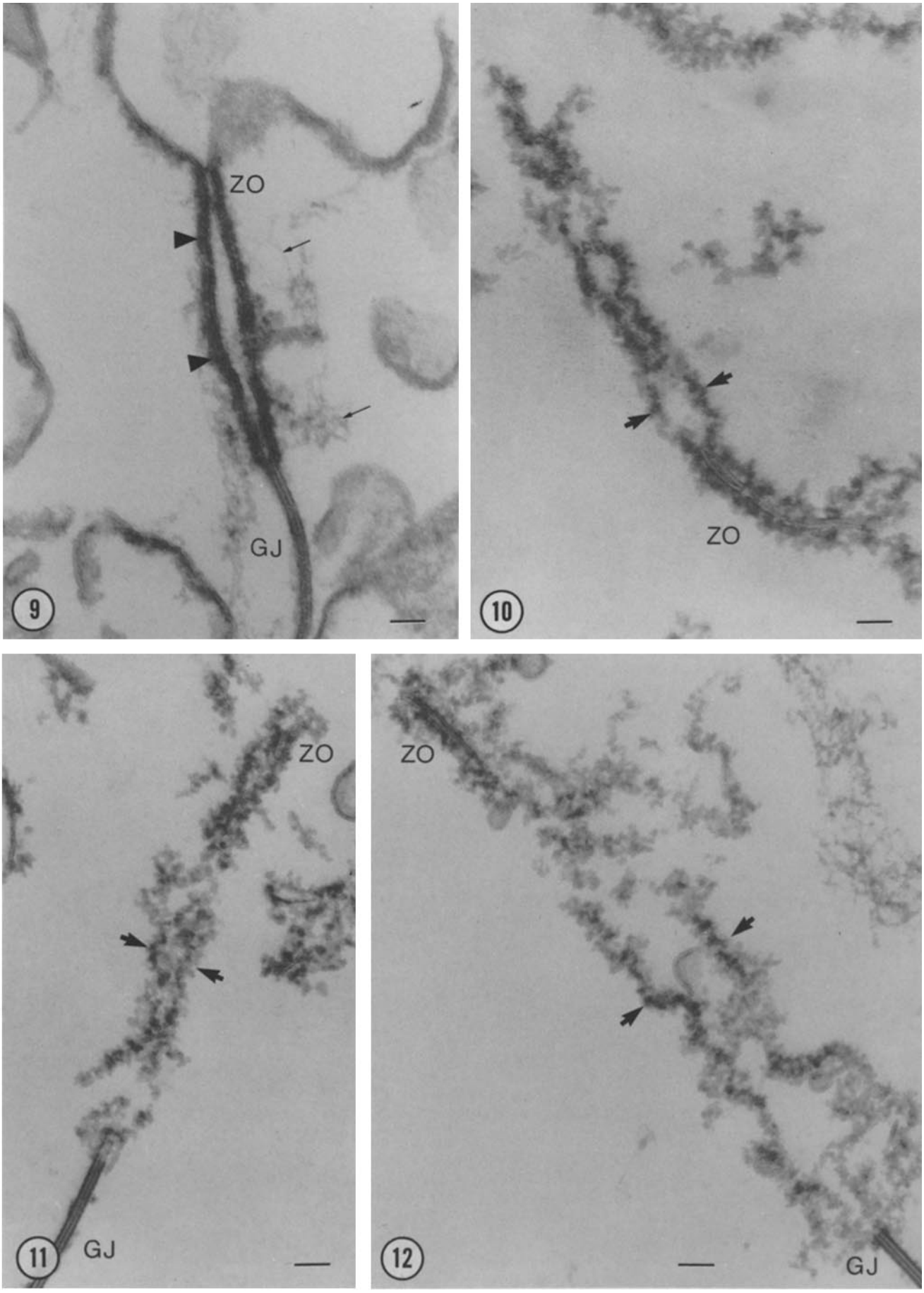
ZO
GJ
9
ZO
10
ZO
GJ
11
ZO
12
GJ

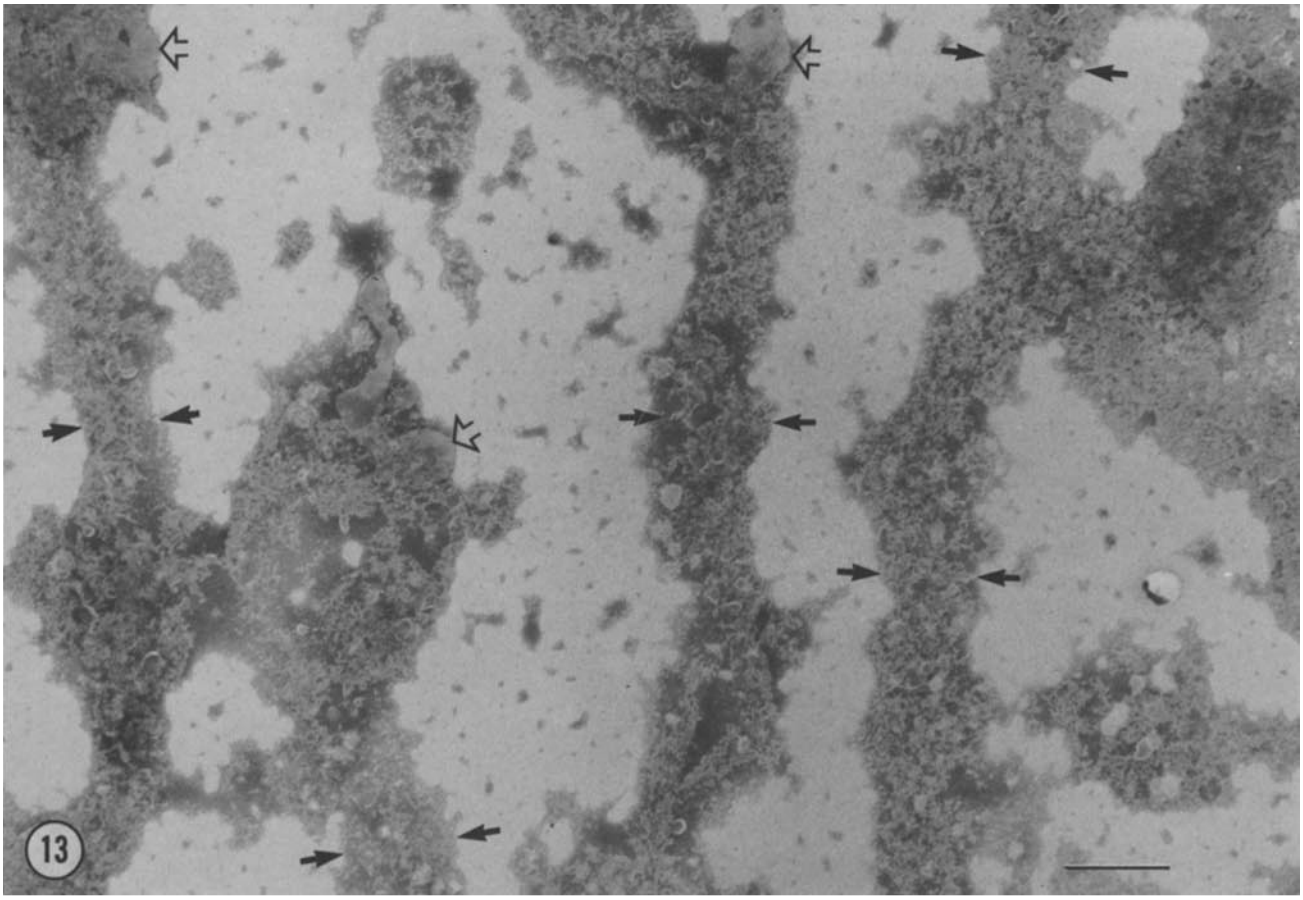
13

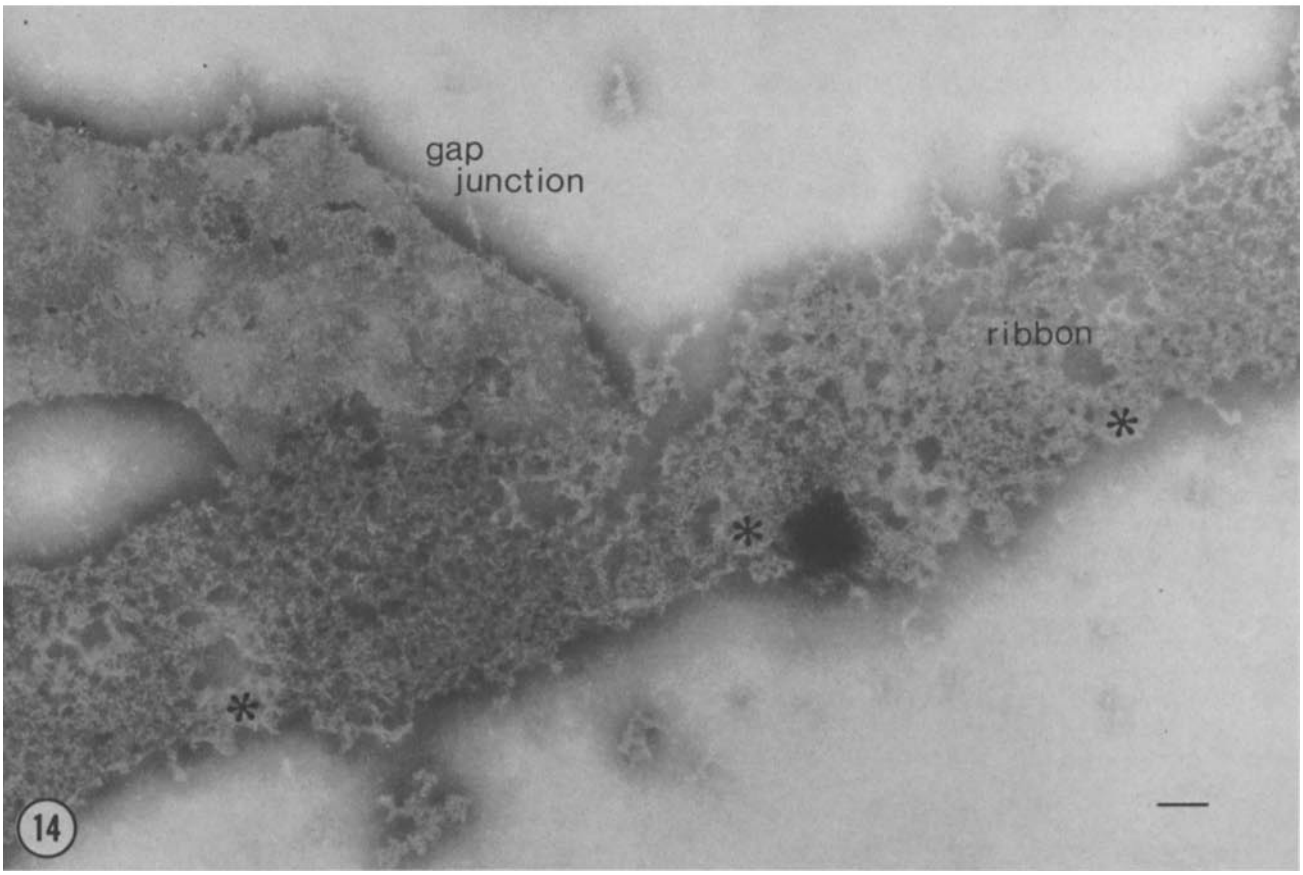
gap
junction
ribbon
14

inar profiles may still be seen in the region of the ZO. In negative stain the residual junctional ribbons dominate the preparation (Fig. 13). High magnification reveals that the texture of the ribbons appears coarser, and that the stain-excluding fibrils seen in the DOC-treated ribbons can no longer be seen (Fig. 14).

Morphometry

Comparison of the freeze-fractured and negatively stained fibril images was made by measuring fibril width and network density (Table I). When negatively stained with K-PT, the mean fibril diameter is 12.5 ± 3.5 nm, and in aqueous UrAc the mean is 14.6 ± 3.5 nm. Freeze-fractured whole liver ZOs show a mean fibril diameter of 12.0 ± 1.8. Although the K-PT and freeze-fracture values are not significantly different ($p = 0.42$), the UrAc diameter is significantly larger than both the K-PT ($p < 0.004$) and freeze-fracture ($p < 0.0001$) values. This difference may in part be due to the lower pH (4.5) of the UrAc staining solution.

Network density, as described by Easter et al. (1983), is the total length of fibril elements divided by the length of the canaliculus bordered by the measured fibril pattern. The values determined for the K-PT and UrAc stained junctional ribbons, 2.17 ± 0.29 and 2.20 ± 0.29, respectively, are not significantly different ($p = 0.84$). However, the network density of the freeze-fractured whole liver ZOs is 3.36 ± 0.66, which is significantly larger than both of the negative stain values (UrAc, $p < 0.0001$; K-PT, $p < 0.004$). During the process of DOC treatment, pieces of fibril may have been lost or solubilized, or the fibril pattern may have become stretched or elongated, resulting in a lower network density for the negatively stained material.

Polyacrylamide Gel Analysis

Prior to DOC treatment, the bile canaliculus-enriched membrane fraction shows a complex protein profile when analyzed on 11% SDS polyacrylamide slab gels (Fig. 15, lane *1*). DOC solubilizes the majority of these polypeptides (lane *2*) and leaves behind the insoluble junctional ribbon fraction shown in lane *3*. It is this material that shows the branching and anastomosing network of fibrils contained within each of the ribbons. The major polypeptides of this DOC-insoluble fraction have molecular weights of 37,000 and 48,000. Distinctive minor bands appear at 34,000, 41,000, 71,000, 86,000, and 102,000, with a doublet at 92,000. The supernatant solution for the SRK treatment is shown in lane *4*, and the SRK-insoluble fraction containing junctional ribbons with

TABLE I

Morphometric Analysis of Freeze-fracture and Negative-stain Images

	Mean fibril diameter	Network density
	nm	
Freeze-fracture	12.0 ± 1.8 (51)*	3.36 ± 0.66 (12)§
Negative stain		
K-PT	12.5 ± 3.5 (51)‡	2.17 ± 0.29 (7)‖
UrAc	14.6 ± 3.5 (51)	2.20 ± 0.29 (10)

* $p = 0.42$, freeze-fracture vs. K-PT; $p < 0.0001$, freeze-fracture vs. UrAc.
‡ $p < 0.004$, K-PT vs. UrAc.
§ $p < 0.004$, freeze-fracture vs. K-PT; $p < 0.0001$, freeze-fracture vs. UrAc.
‖ $p = 0.84$, K-PT vs. UrAc.

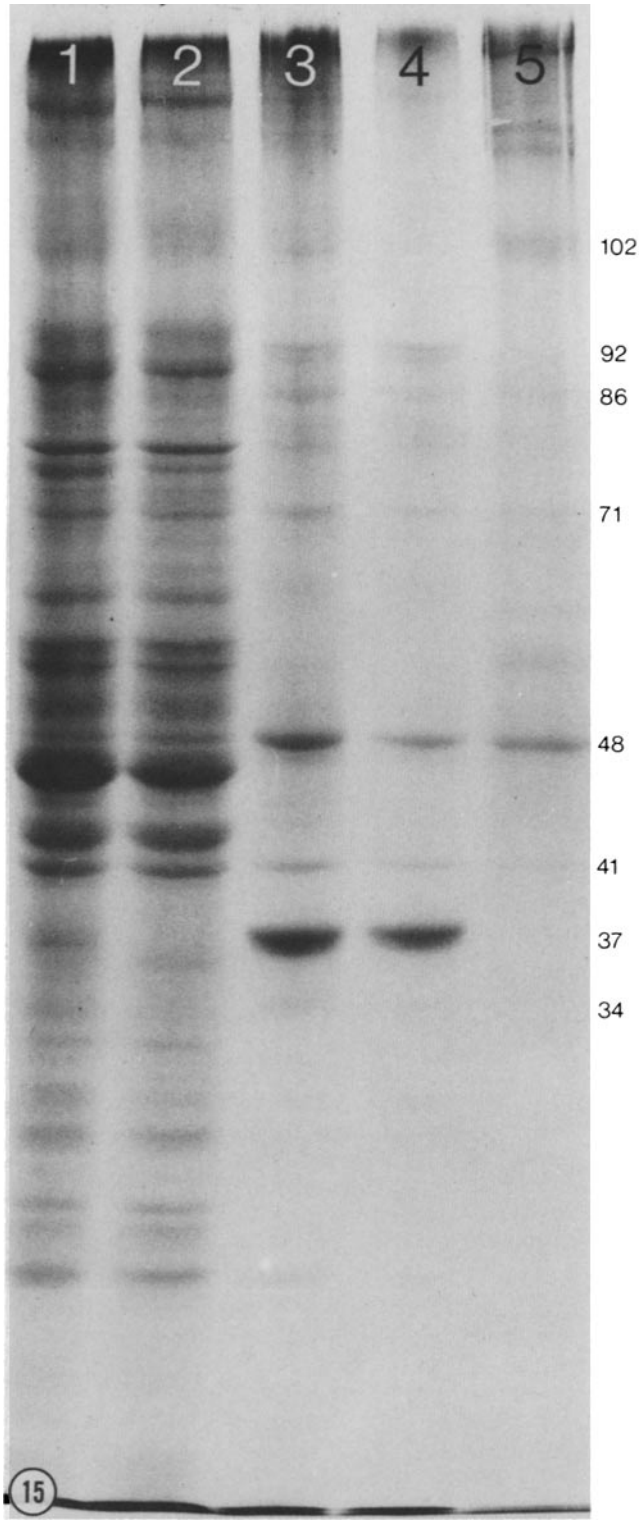

FIGURE 15 11% SDS-polyacrylamide gel of proteins from liver isolation protocol fractions. Lane *1*, bile canaliculus-enriched fraction prior to detergent treatment. (See Figs. 3 and 9; 5 μl loaded.) Lane *2*, proteins solubilized by treatment with DOC (10 μl); lane *3*, DOC-insoluble fraction. It is this fraction that shows the branching and anastomosing fibrils in the negatively stained junctional ribbons. Major bands appear at 37,000 and 48,000, with minor bands at 34,000, 41,000, 71,000, 86,000, 92,000, and 102,000. (See Figs. 5–8, 10, 11; 10 μl.) Lane *4*, proteins solubilized by treatment with SRK (10 μl); lane *5*, SRK-insoluble fraction. This fraction contains the junctional ribbons in which the fibrils are no longer visible. (See Figs. 12–14; 20 μl.)

the altered texture is profiled in lane 5. The same SRK treatment that causes the fibrils to disappear from the negatively stained junctional ribbons partially releases the 41,000, 48,000, 71,000, and 86,000 M_r polypeptides, whereas the 34,000 and the 37,000 M_r proteins, and the doublet at 92,000 move quantitatively from the pellet to the supernatant solution.

We would like to emphasize strongly the preliminary nature of these SDS polyacrylamide gels. The results are presented here only to provide a framework for comparison between our results and those produced in other laboratories. The definitive assignment of a specific polypeptide to any structure within the junctional complex, let alone the ZO itself, is well in the future.

DISCUSSION

Morphology of the Isolated Preparations

This paper presents a protocol for the isolation of an enriched preparation of junctional complexes from mouse liver, using detergent solubilization in conjunction with subcellular fractionation techniques. These junctional complexes contain the structural components of ZOs as judged by morphological criteria. The classic liver plasma membrane preparation of Neville (1960), as modified by Emmelot et al. (1964) and Song et al. (1969), contains numerous bile canaliculi with associated junctional complexes. Treatment of this preparation with EGTA and DOC results in a solubilization of the bile canalicular, organellar, and lateral plasma membranes, leaving gap junctions, collagen, and long ribbon-like remnants of the junctional complexes. Goodenough and Revel (1970) demonstrated that a branching and anastomosing network of fibrils, characteristic of the freeze-fracture appearance of the ZO, could be visualized as stain-excluding structures both in negative stain (K-PT) of a similar liver plasma membrane fraction treated with DOC, and in acetone-treated lanthanum-stained whole liver (see Figs. 9 and 15, reference 25). In our enrichment protocol, this view of the ZO fibrils is preserved in junctional ribbons following extensive washing with EGTA and DOC.

Measurements of fibril diameter and network density in both the negative stain and freeze-fracture specimens indicate a similarity between these images. As revealed by statistical analysis, the mean fibril diameter of 12.5 ± 3.5 nm for K-PT staining and 12.0 ± 1.8 nm for freeze-fracture are not significantly different, while that for UrAc, at 14.6 ± 3.5, is significantly larger. This difference may be due to the fact that UrAc staining solution is pH 4.5, well below that of K-PT (pH 7.0) and that which whole liver cells are exposed to prior to freezing. This lower pH may cause the fibrils to swell, or may change some fibril property that results in a wider area of stain exclusion. Alternatively, the lowered pH may result in the solubilization of some fibril constraint, allowing them to move about more freely. This movement may result in fibrils lying side-by-side, yielding more double fibril images, as seen in Fig. 8. Inclusion of these double fibrils in measurements would skew the data toward a larger mean diameter.

The network density determined for the freeze-fractured whole mouse liver ZOs is significantly larger than that for the fibril pattern visualized either in K-PT- or UrAc-stained junctional ribbons. Segments of the fibrils may be lost during the isolation procedure, or released when the surrounding membrane is solubilized by DOC treatment. Alternatively, the ZOs may become stretched or elongated during the isolation, detergent extraction, or negative staining processes (34), resulting in a lower network density. Easter et al. (1983) found a network density of 5.36 ± 0.79 for freeze-fractured rat liver ZOs, a value somewhat higher than that obtained here for freeze-fractured mouse liver (see Table I). The reason for this difference is not known, although it may be related to a species variation.

The geometric relationship between the fibrils seen by negative staining and freeze-fracture electron microscopy is not clear. Current interpretations hold that during the fracturing process membranes split in the center of the bilayer (4, 48); hence the ZO fibrils seen in freeze-fracture would be intramembrane structures (5, 57, 62). Due to the loss of the membrane lipid continuum in the DOC-treated junctional ribbons, it has not yet been possible to obtain fracture faces of this material that demonstrate the fibril network. Since the negatively stained fibrils are viewed in projection, there is no information as to their position within the junctional profile. Thus it is not known if the negatively stained and freeze fracture fibrils are identical or related structures. Because the only assay for the ZOs in the liver preparations is morphological, it is not possible to reach any conclusions regarding the functional integrity of these isolated ZOs. It is possible that components integral to normal ZO physiology have been lost during the isolation and extraction process.

Composition of the ZO Fibrils

Recent studies by Griepp et al. (1983 [30]) demonstrated that trypsinized MDCK cells were unable to form ZOs when plated in the presence of cycloheximide. Staehelin (1973 [57]) and van Deurs and Luft (1979 [61]) have shown that in freeze-fracture replicas the ZO fibril appeared as a series of individual intramembranous particles in unfixed material. As glutaraldehyde is primarily a protein cross-linker, these investigators concluded that the basic component of the ZO is proteinaceous in nature. Recently, however, an alternative model has been presented. In the absence of glutaraldehyde fixation, "optimal" quick-freezing conditions revealed prostate gland ZO fibrils to be continuous and not a string of individual intramembranous particles (35). These observations led to the hypothesis that the ZO is composed of an inverted cylindrical lipid micelle lying with its long axis parallel to the plane of the membrane (35, 49). In a different tissue, rabbit ciliary epithelium, Raviola et al. (1980 [50]) used quick-freezing methodology to show that the ZO appeared as discontinuous fibrils or a linear series of particles, similar to those reported by Staehelin (1973). These data may indicate that ZOs are a heterogeneous class of intercellular junctions, and may therefore display different fracturing properties in different tissues. Indeed, different fracturing properties have been noted between fixed ZOs as well (8).

The fibrils visualized in our negatively-stained junctional ribbons were structurally resistant to treatment with DOC, an anionic detergent that would be expected to destroy lipid structural domains. These fibrils were structurally sensitive to treatment with SRK, another anionic detergent. In addition, the ZOs present in isolated brush borders appear in thin section to be structurally resistant to treatment with 2.0% Triton X-100, a nonionic detergent (58), although individual fibrils were not visualized in this study. The concentrations of detergents used during these extractions are significantly

above the critical micellar concentration. However, because we have been unable to visualize whole fibril networks in freeze-fracture replicas of these detergent-treated samples, we are unable to critically test the hypothesis (35, 49) that the freeze-fracture fibrils are inverted lipid micelles. All we can conclude at the present time is that there are detergent-resistant fibrils contained within the negatively-stained junctional ribbons, similar in size and geometry to freeze-fractured ZOs, which may correspond directly or indirectly (e.g., a cytoplasmic scaffolding) to the freeze-fractured fibrils.

The Role of Calcium in ZO Structure

Previous reports in the literature have indicated that calcium plays a role in the stabilization of ZO structure (7, 9, 21, 31, 42, 43, 51). Sedar and Forte (51), using whole gastric mucosa mounted in an Ussing chamber for electrophysiological measurements, showed that within 15 min of exposure of both epithelial surfaces to 4.0 mM EDTA there was a significant drop in transmucosal resistance, a parameter determined largely by the paracellular pathway. Cereijido et al. (1978 [7]), using the transporting epithelial cell line MDCK, observed a similar drop in transepithelial resistance in response to 2.5 mM EGTA. This effect was reversible upon readdition of calcium. These authors also noted an EGTA-induced separation of ZO membranes in thin section. Meldolesi et al. (1978 [43]) observed a reversible disruption of the freeze-fracture ZO fibril pattern in pancreatic acinar cells upon treatment with 0.5 mM EGTA.

In an isolated form in our fractions, the liver ZO maintains its characteristic morphology in the presence of millimolar concentrations of EGTA. Thin sections of the isolated liver junctions show that the ZO appears as a series of punctate fusions of the outer leaflet of the plasma membrane, the same as it appears in the whole tissue. In addition, this appearance is stable to exposure to 1 mM EGTA at 37°C for 30 min, the longest time tested (data not shown). Further evidence for the stability of this structure in the presence of calcium chelators comes from the fact that the branching and anastomosing pattern of fibrils seen in freeze-fracture of the whole liver can also be visualized in freeze-fracture of EGTA-treated isolated membranes and in negatively stained EGTA- and DOC-treated junctional ribbons. These results indicate that in intact cells the ultrastructural changes observed in the ZO following calcium chelation are not due directly to removal of calcium, but are the result of secondary cellular responses. The physiological decrease in paracellular resistance induced by low extracellular calcium may involve alterations in the 1–2-nm diam transjunctional channels (45, 46). Changes in structure at this level would not be detected in this study.

Biochemical Characterization

When analyzed on SDS-polyacrylamide slab gels, the DOC-insoluble junctional ribbons show a relatively simple gel profile, with major bands at 37,000 and 48,000 and minor bands at 34,000, 41,000, 71,000, 86,000, and 102,000, with a doublet at 92,000. Upon extraction with SRK, a fraction of each of the 41,000, 48,000, 71,000, and 86,000 M_r polypeptides appear in the SRK supernatant solution, whereas the 34,000 and 37,000 M_r protein, and the doublet at 92,000 move quantitatively from the SRK-insoluble pellet to the supernatant solution. The same SRK treatment also causes the fibrils to disappear from the junctional ribbons. This suggests that one or more of those proteins present in the SRK supernatant solution may play a role in the maintenance of fibril structure. It is also possible that the absence of fibrils in the SRK-treated junctional ribbons is due to a detergent-induced molecular rearrangement of fibril components and not a solubilization, so it cannot be conclusively stated that any of those peptides found in the SRK supernatant solution represents the fibrils themselves. Comparison of the amount of actual fibril material with the amount of the cytoplasmic density in which the fibrils are embedded indicates that the fibrils should be a relatively minor component of our preparation. The large amount of the 37,000 M_r band present, despite its quantitative appearance in the SRK supernatant solution, makes it unlikely that the fibrils are composed of this polypeptide.

Very little is known about the nature of the junctional complex-associated cytoplasmic density that comprises the bulk of the DOC-extracted junctional ribbons. Desmosomes have "attachment plaques" applied to the cytoplasmic surfaces of the junctional membranes that have been demonstrated to be partially composed of the 250,000 and 215,000 M_r "desmoplakins" (17). We find material of this molecular weight on our gels of junctional ribbons, although these peptides are not major components, and hence are unlikely to correspond to the cytoplasmic density seen on the junctional ribbons.

Homogeneous preparations of desmosomes have been isolated and their biochemical components partially characterized (10, 29, 52, 53). Extraction of these isolated desmosomes with metrizamide gradients (29) or low ionic strength solutions (54) resulted in reduction of the attachment plaque material and the loss or diminution of a variety of peptides, including ones of 90,000 (54) and 86,000 M_r, and an enrichment of proteins thought to participate in intercellular adhesion in the desmosomal cores, including one at 100,000 M_r (29). These polypeptides may correspond to the 102,000, 92,000, and 86,000 M_r bands seen in the DOC-insoluble junctional ribbon fraction. Vinculin, a 130,000 M_r protein found in regions where microfilament bundles terminate at membranes, and alpha-actinin (95,000 M_r), another protein known to interact with microfilaments, have been localized by immunoelectron microscopy of frozen thin sections to the zonula adhaerens membrane region. No activity was seen in association with either the desmosome or the ZO (22–24). Bands of this molecular weight are not detectable in the Coomassie Blue-stained gels presented here. Very little of the 28,000 M_r peptide associated with hepatocyte gap junctions (32, 33) is visible on these gels, indicating that gap junctions are a relatively minor contaminant. Using antisera generated against the DOC-insoluble fraction, we are in the process of affinity-purifying antibodies to the various protein components present in the junctional ribbons, and localizing these activities with the ZO structure using immunocytochemistry.

We would like to thank Drs. Mark S. Mooseker and David L. Paul for their invaluable gifts of time, encouragement, assistance, and friendship.

This research is supported by grant GM 28932 from the National Institutes of Health.

Received for publication 24 May 1983, and in revised form 20 October 1983.

REFERENCES

1. Begg, D. A., R. Rodewald, and L. I. Rebhun. 1978. The visualization of actin filament polarity in thin sections. Evidence for uniform polarity of membrane-associated filaments. *J. Cell Biol.* 79:846–852.
2. Benedetti, E. L., and P. Emmelot. 1968. Hexagonal array of subunits in tight junctions separated from isolated rat liver plasma membranes. *J. Cell Biol.* 38:15–24.
3. Berry, M. N., and D. S. Friend. 1969. High-yield preparation of isolated rat liver parenchymal cells. A biochemical and fine structure study. *J. Cell Biol.* 43:506–520.
4. Branton, D. 1966. Fracture faces of frozen membranes. *Proc. Natl. Acad. Sci. USA.* 55:1048–1056.
5. Bullivant, S. 1978. The structure of tight junctions. *In* Ninth International Congress on Electron Microscopy. 659–672.
6. Cassidy, M. M., and C. S. Tidball. 1967. Cellular mechanism of intestinal permeability alterations produced by chelation depletion. *J. Cell Biol.* 32:685–698.
7. Cereijido, M., E. S. Robbins, W. J. Dolan, C. A. Rotunno, and D. D. Sabatini. 1978. Polarized monolayers formed by epithelial cells on permeable and translucent support. *J. Cell. Biol.* 77:853–880.
8. Claude, P., and D. A. Goodenough. 1973. Fracture faces of zonulae occudentes from "tight" and "leaky" junctions. *J. Cell Biol.* 58:390–400.
9. Curran, P. F., J. Zadunaisky, and J. R. Gill, Jr. 1961. The effect of ethylenediaminetetraacetate on ion permeability of the isolated frog skin. *Biochim. Biophys. Acta.* 52:392–395.
10. Drochmans, P., C. Freudenstein, J. C. Wanson, L. Laurent, T. W. Keenen, J. Stadler, R. Leloup, and W. W. Franke. 1978. Structure and biochemical composition of desmosomes and tonofilaments isolated from calf muzzle epidermis. *J. Cell Biol.* 79:427–443.
11. Dunia, I., C. S. Ghosh, and E. L. Benedetti. 1974. Isolation and protein pattern of eye lens fiber junctions. *FEBS (Fed. Eur. Biol. Soc.) Lett.* 45:139–144.
12. Easter, D. W., J. B. Wade, and J. L. Boyer. 1983. Structural integrity of hepatocyte tight junctions. *J. Cell Biol.* 96:745–749.
13. Emmelot, P., C. J. Bos, E. L. Benedetti, and P. H. Rumke. 1964. Studies on plasma membranes. I. Chemical composition and enzyme content of plasma membranes isolated from rat liver. *Biochim. Biophys. Acta.* 90:126–145.
14. Fairbanks, G., T. L. Steck, and D. F. H. Wallach. 1971. Electrophoretic analysis of the major polypeptides of the human erythrocyte membrane. *Biochemistry.* 10:2606–2617.
15. Farquhar, M. G., and G. E. Palade. 1963. Junctional complexes in various epithelia. *J. Cell Biol.* 17:375–412.
16. Forte, J. G., and A. H. Nauss. 1963. Effects of calcium removal on bullfrog gastric mucosa. *Am. J. Physiol.* 205:631–637.
17. Franke, W. W., R. Moll, D. L. Schiller, E. Schmid, J. Kartenbach, and H. Mueller. 1982. Desomoplakins of epithelial and myocardial desmosomes are immunologically and biochemically related. *Differentiation.* 23:115–127.
18. Friend, D. S., and N. B. Gilula. 1972. Variations in tight and gap junctions in mammalian tissues. *J. Cell Biol.* 53:758–776.
19. Frömter, E. E. 1972. The route of passive ion movement through the epithelium of Necturus gallbladder. *J. Membr. Biol.* 8:259–301.
20. Frömter, E., and J. Diamond. 1972. Route of passive ion permeation in epithelia. *Nature (Lond.).* 235:9–13.
21. Galli, P., A. Brenna, P. DeCamilli, and J. Meldolesi. 1976. Extracellular calcium and the organization of tight junctions in pancreatic acinar cells. *Exp. Cell Res.* 99:178–183.
22. Geiger, B., K. T. Tokuyasu, and S. J. Singer. 1979. Immunocytochemical localization of alpha-actinin in intestinal epithelial cells. *Proc. Natl. Acad. Sci. USA.* 76:2833–2837.
23. Geiger, B., K. T. Tokuyasu, A. H. Dutton, and S. J. Singer. 1980. Vinculin, an intracellular protein localized at specialized sites where microfilament bundles terminate at cell membranes. *Proc. Natl. Acad. Sci. USA.* 77:4127–4131.
24. Geiger, B., A. H. Dutton, K. T. Tokuyasu, and S. J. Singer. 1981. Immunoelectron microscope studies of membrane-microfilament interactions: distributions of alpha-actinin, tropomyosin, and vinculin in intestinal epithelial brush border and chicken gizzard smooth muscle cells. *J. Cell Biol.* 91:614–628.
25. Goodenough, D. A., and J. P. Revel. 1970. A fine structural analysis of the intercellular junctions in the mouse liver. *J. Cell Biol.* 45:272–290.
26. Goodenough, D. A., and W. Stoeckenius. 1972. The isolation of mouse hepatocyte gap junctions. Preliminary chemical characterization and X-ray diffraction. *J. Cell Biol.* 54:646–656.
27. Goodenough, D. A. 1975. Methods for the isolation and structural characterization of hepatocyte junctions. *In* Methods in Membrane Biology. E. D. Korn, editor. Plenum Publishing Corp., New York.
28. Goodenough, D. A. 1979. Lens gap junctions: a structural hypothesis for non-regulated low-resistance intercellular pathways. *Invest. Ophthalmol. Visual Sci.* 18:1104–1122.
29. Gorbsky, G., and M. S. Steinberg. 1981. Isolation of the intercellular glycoproteins of desmosomes. *J. Cell Biol.* 90:243–248.
30. Griepp, E. B., W. J. Dolan, E. S. Robbins, and D. D. Sabatini. 1983. Participation of plasma membrane proteins in the formation of tight junctions by cultured epithelial cells. *J. Cell Biol.* 96:693–702.
31. Hays, R. M., B. Singer, and S. Malamed. 1965. The effect of calcium withdrawl on the structure and function of the toad bladder. *J. Cell Biol.* 25:195–208.
32. Henderson, D., H. Eibl, and K. Weber. 1979. Structure and biochemistry of mouse hepatic gap junctions. *J. Mol. Biol.* 132:193–218.
33. Hertzberg, E. L., and N. B. Gilula. 1979. Isolation and characterization of gap junctions from rat liver. *J. Biol. Chem.* 254:2138–2147.
34. Hull, B. E., and L. A. Staehelin. 1976. Functional significance of the variations in the geometrical organization of tight junction networks. *J. Cell Biol.* 68:688–704.
35. Kachar, B., and T. S. Reese. 1982. Evidence for the lipidic nature of tight junction strands. *Nature (Lond.).* 296:464–466.
36. Karnovsky, M. J. 1965. A formaldehyde-glutaraldehyde fixative of high osmolarity for use in electron microscopy. *J. Cell Biol.* 27:137*a*. (Abstr.)
37. Karnovsky, M. J. 1971. Use of ferrocyanide-reduced osmium tetroxide in electron microscopy. Abstracts of Papers, 11th Annual Meeting, The American Society for Cell Biology. 146.
38. Kensler, R. W., and D. A. Goodenough. 1980. Isolation of mouse myocardial gap junctions. *J. Cell Biol.* 86:755–764.
39. Kreutziger, G. O. 1968. Freeze-etching of intercellular junctions of mouse liver. *In* Proceedings of the 26th Annual Meeting of the Electron Microscopy Society of America. 234–235.
40. Laemmli, U. K. 1970. Cleavage of structural proteins during the assembly of the head of bacteriophage T4. *Nature (Lond.).* 227:680–685.
41. Lowry, O. H., N. J. Rosebrough, A. L. Farr, and R. J. Randall. 1951. Protein measurement with the Folin phenol reagent. *J. Biol. Chem.* 193:265–275.
42. Martinez-Palomo, A., I. Meza, G. Beaty, and M. Cereijido. 1980. Experimental modulation of occluding junctions in a cultured transporting epithelium. *J. Cell Biol.* 87:736–745.
43. Meldolesi, J., G. Castiglioni, R. Parma, N. Nassivera, and P. DeCamilli. 1978. Calcium-dependent disassembly and reassembly of occluding junctions in guinea pig pancreatic acinar cells. Effects of drugs. *J. Cell Biol.* 79:156–172.
44. Miller, F. 1960. Hemoglobin absorption by the cells of the proximal convoluted tubule in mouse kidney. *J. Biophys. Biochem. Cytol.* 8:689–718.
45. Moreno, J. H., and J. M. Diamond. 1974. Discrimination of monovalent inorganic cations by "tight" junctions of gallbladder epithelium. *J. Membr. Biol.* 15:277–318.
46. Moreno, J. H., and J. M. Diamond. 1975. Nitrogenous cations as probes of permeation channels. *J. Membr. Biol.* 21:197–259.
47. Neville, D. M. 1960. The isolation of a cell membrane fraction from rat liver. *J. Biophys. Biochem. Cytol.* 8:413–422.
48. Pinto da Silva, P., and D. Branton. 1970. Membrane splitting in freeze-etching: covalently bound ferritin as a membrane marker. *J. Cell Biol.* 45:598–605.
49. Pinto da Silva, P., and B. Kachar. 1982. On tight-junction structure. *Cell.* 28:441–450.
50. Raviola, E., D. A. Goodenough, and G. Raviola. 1980. Structure of rapidly frozen gap junctions. *J. Cell Biol.* 87:273–279.
51. Sedar, A. W., and J. G. Forte. 1964. Effects of calcium depletion on the junctional complex between oxyntic cells of gastric mucosa. *J. Cell Biol.* 22:173–188.
52. Skerrow, C. J., and A. G. Matoltsy. 1974. Isolation of epidermal desmosomes. *J. Cell Biol.* 63:515–523.
53. Skerrow, C. J., and A. G. Matoltsy. 1974. Chemical characterization of isolated epidermal desmosomes. *J. Cell Biol.* 63:524–530.
54. Skerrow, C. J. 1979. Selective extraction of desmosomal proteins by low ionic strength media. *Biochim. Biophys. Acta.* 579:241–245.
55. Song, C. S., W. Rubin, A. B. Rifkind, and A. Kappas. 1969. Plasma membranes of the rat liver. Isolation and enzymatic characterization of a fraction rich in bile canaliculi. *J. Cell Biol.* 41:124–132.
56. Staehelin, L. A., T. M. Mukherjee, and A. W. Williams. 1969. Freeze-etch appearance of the tight junctions in the epithelium of small and large intestine of mice. *Protoplasma.* 67:165–184.
57. Staehelin, L. A. 1973. Further observations on the fine structure of freeze-cleaved tight junctions. *J. Cell Sci.* 13:763–786.
58. Stevenson, B. R., D. A. Goodenough, and M. S. Mooseker. 1982. Zonulae occludentes in plasma membrane fractions from chicken intestine and mouse liver. *J. Cell Biol.* 95:92*a*. (Abstr.)
59. Teillet, M. A., J. S. Hugon, and R. Calvert. 1981. The occluding junctions of mouse duodenal enterocytes during development. A freeze-fracture study. *Cell Tiss. Res.* 217:65–77.
60. van Deurs, B., and J. K. Koehler. 1979. Tight junctions in the choroid plexus epithelium. A freeze-fracture study including complimentary replicas. *J. Cell Biol.* 80:662–673.
61. van Deurs, B., and J. H. Luft. 1979. Effects of glutaraldehyde fixation on the structure of tight junctions. A quantitative freeze-fracture analysis. *J. Ultrastruct. Res.* 68:160–172.
62. Wade, J. B., and M. J. Karnovsky. 1974. The structure of the zonula occludens. A single fibril model based on freeze-fracture. *J. Cell Biol* 60:168–180.